THE JOURNAL OF PHYSICAL CHEMISTRY C

Article

pubs.acs.org/JPCC

# Probing Transient Valence Orbital Changes with Picosecond Valence-to-Core X-ray Emission Spectroscopy

Anne Marie March,[*,†] Tadesse A. Assefa,[‡] Christina Boemer,[‡,¶] Christian Bressler,[‡,¶,§] Alexander Britz,[‡,¶] Michael Diez,[‡,¶] Gilles Doumy,[†] Andreas Galler,[‡] Manuel Harder,[∥] Dmitry Khakhulin,[‡,¶] Zoltán Németh,[⊥] Mátyás Pápai,[⊥,@] Sebastian Schulz,[‡,¶] Stephen H. Southworth,[†] Hasan Yavaş,[∥] Linda Young,[†,Δ] Wojciech Gawelda,[*,‡,▽] and György Vankó[*,⊥]

[†]Chemical Sciences and Engineering Division, Argonne National Laboratory, Argonne, Illinois 60439, United States

[‡]European XFEL, Holzkoppel 4, D-22869 Schenefeld, Germany

[¶]The Hamburg Centre for Ultrafast Imaging, Luruper Chaussee 149, 22761 Hamburg, Germany

[§]Department of Physics, Technical University of Denmark, Fysikvej 307, DK-2800, Kongens Lyngby, Denmark

[∥]Deutsches Elektronen-Synchrotron (DESY), 22607 Hamburg, Germany

[⊥]Wigner Research Centre for Physics, Hungarian Academy Sciences, H-1525 Budapest, Hungary

[@]Department of Chemistry, Technical University of Denmark, Kemitorvet 207, DK-2800, Kongens Lyngby, Denmark

[Δ]Department of Physics and James Franck Institute, The University of Chicago, Chicago, Illinois 60637, United States

[▽]Institute of Physics, Jan Kochanowski University, 25-406 Kielce, Poland

**ABSTRACT:** We probe the dynamics of valence electrons in photoexcited $[Fe(terpy)_2]^{2+}$ in solution to gain deeper insight into the Fe−ligand bond changes. We use hard X-ray emission spectroscopy (XES), which combines element specificity and high penetration with sensitivity to orbital structure, making it a powerful technique for molecular studies in a wide variety of environments. A picosecond-time-resolved measurement of the complete 1s X-ray emission spectrum captures the transient photoinduced changes and includes the weak valence-to-core (vtc) emission lines that correspond to transitions from occupied valence orbitals to the nascent core-hole. Vtc-XES offers particular insight into the molecular orbitals directly involved in the light-driven dynamics; a change in the metal−ligand orbital overlap results in an intensity reduction and a blue energy shift in agreement with our theoretical calculations and more subtle features at the highest energies reflect changes in the frontier orbital populations.

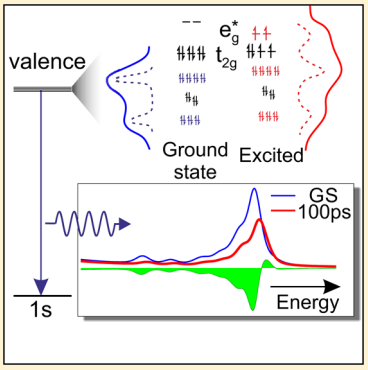


## INTRODUCTION

Valence-to-core X-ray emission spectroscopy (vtc-XES) is an emerging, information-rich technique to characterize chemically active metal sites,[1−4] which has started to fully unfold its potential only recently, after its theoretical modeling became readily available.[5−10] The features in this hard X-ray spectral region stem from radiative transitions from occupied valence orbitals to an inner core-hole vacancy generated, for instance, through X-ray absorption by a core electron. The transition probability can be about 3 orders of magnitude lower than that of the main emission lines (e.g., 2p → 1s) and is therefore challenging to measure. With the high X-ray flux provided by modern synchrotron sources (and emerging X-ray free electron lasers) measurement of vtc-XES is possible even for dilute samples. The chemical information content has been elucidated by several experimental and theoretical studies.[1−10] The interpretation of spectral features is facilitated by the fact that simple electric dipole transitions dominate the spectra. In 3d transition metal compounds vtc-XES is particularly sensitive to the ligands coordinating the metal ion, including the number and distance.[1] One can also determine the type of molecules bound to the metal and detect chemical changes in ligands such as protonation.[3,8,9,11] The intensity of vtc-XES features can be used to indicate bond activation of ligands,[12] and studies of bioinorganic molecules[7,13] next to in situ and in operando studies of catalysts[4,10,14,15] demonstrate the technique's applicability to rather complex sample environments.

We extend here vtc-XES to the ultrafast time domain, an important step toward the aim of watching the evolution of valence electrons during the course of a chemical reaction. Our measurement captures the short-lived high-spin (HS) excited state of an Fe(II)-based polypyridal complex, $[Fe(terpy)_2]^{2+}$ (terpy =2,2′:6′,2″-terpyridine), in an aqueous solution. The low-spin (LS) ground state, with a $(t_{2g})^6$ configuration for the Fe 3d valence electrons (approximating octahedral symmetry for simplicity), is switched to the HS state, with $(t_{2g})^4(e_g^*)^2$ configuration, via ultrashort laser pulse excitation in the visible

**Received:** December 23, 2016
**Published:** January 17, 2017




DOI: 10.1021/acs.jpcc.6b12940
J. Phys. Chem. C 2017, 121, 2620−2626

regime. The photoabsorption initially excites a metal-to-ligand charge transfer (MLCT) manifold of states which undergoes internal conversions and intersystem crossings to the lowest metal-centered high spin (HS) quintet excited state in <1 ps.[16,17] The HS state decays nonradiatively back to the LS ground state with a lifetime of 2.6 ns in room-temperature aqueous solution.[18]

## EXPERIMENTAL AND THEORETICAL METHODS

**Experimental Details.** Figure 1 depicts the laser-pump/X-ray-probe measurement scheme. The low vtc-XES yield required both a very efficient use of the incident X-ray flux and efficient collection of the X-ray fluorescence. The former was secured by pump−probe cycles at the same MHz repetition rate of the X-rays and the latter with a 16-crystal dispersive spectrometer that covered a large solid angle. Complete Fe 1s emission spectra were collected using eight of the crystals to diffract the K$\alpha$ (2p → 1s) lines and the other eight to diffract the mainline K$\beta$ (3p → 1s) and vtc emission lines.

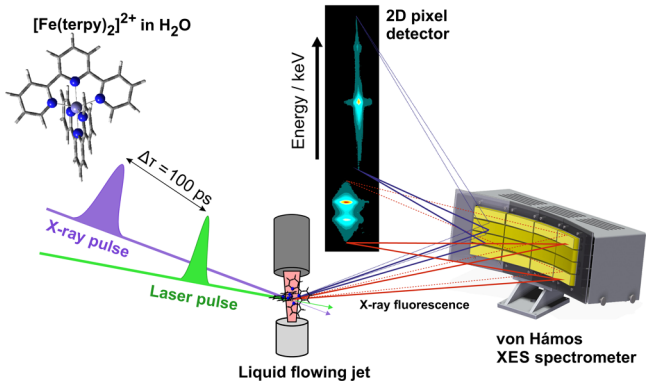


**Figure 1.** Experimental setup showing the 16-crystal von Hamos spectrometer installed at 7ID-D in a pump−probe geometry. Two different sets of eight Si analyzer crystals were used to collect both K$\alpha$ and K$\beta$ plus vtc X-ray emission simultaneously. The detector image shown is a cropped actual frame from the Pilatus 100k pixel detector recorded during the experiment. On the left, the molecular structure of the $[Fe(terpy)_2]^{2+}$ complex is shown.

Measurements were carried out at 7ID-D at the Advanced Photon Source[19] using the high-repetition-rate pump−probe liquid-jet setup developed there.[20−22] Microfocused X-rays spatially overlapped the pump laser with a 100 ps relative delay at a flat liquid jet, and fluorescence from the sample was collected and spectrally resolved using a multicrystal emission spectrometer in the von Hamos geometry. The spectrometer, built by JJ X-ray (www.jjxray.dk) for the FXE beamline at the European XFEL,[23] consists of 16 cylindrically bent crystals, each of which is secured to a kinematic mount that is individually adjustable using three actuators driven by stepper motors. The design is adapted from the spectrometer built by R. Alonso Mori and U. Bergmann for the SSRL and LCLS.[24] Eight of the crystals were segmented Si(111) analyzers, made at the Paul Scherrer Institute, and were used to measure the K$\alpha$ region of the emission spectrum. The other eight crystals were single crystal Si(220) analyzers purchased from Saint-Gobain Crystals (www.crystals.saint-gobain.com) and used to measure the K$\beta$ and valence-to-core region of the spectrum. The crystals were each 30 mm × 110 mm (in the dispersive and focusing directions, respectively), pressed on cylindrical substrates with curvature (50 cm radius) along the direction orthogonal to the dispersion plane. The spectrometer was positioned at 90° relative to the incident X-ray beam to reduce contribution from elastic scattering. The crystals directed the focused and energy-dispersed fluorescence onto a 2D hybrid pixel array detector (Pilatus 100k, Dectris) that was positioned above the liquid jet. The vertical dispersion is advantageous because the source size (X-ray probed region along the liquid jet) does not impact the spectral resolution. A helium bag was used to encompass the path from the sample, to the analyzer crystals, and to the detector. For both K$\alpha$ and K$\beta$, the spectrometer resolution was ∼0.6 eV. The resolution was due to the pixel size of the detector, 172 $\mu$m, corresponding to 0.4 eV (0.5 eV) for K$\alpha$ (K$\beta$), and the misalignment in the overlapping of the analyzer crystals (0.3−0.4 eV). Scans around the elastic lines with ∼0.4 eV bandwidth of the incident X-rays resulted in 0.7−0.8 eV FWHMs, in agreement with the above.

The sample consisted of a 250 mL, 20 mM $[Fe(terpy)_2]^{2+}$ solution in water. It was circulated through a sapphire nozzle that produced a flat, 100 $\mu$m thick jet. The jet was oriented at an angle of ≈45° with respect to the incident X-ray beam to enable a clear path for the X-ray emission to the crystal analyzers.

The X-ray flux on the sample was $2 \times 10^{12}$ photons/second corresponding to $3 \times 10^5$ photons/pulse. The X-rays, centered at 7.4 keV (above the Fe K-edge at 7.112 keV), were monochromatized using a double crystal diamond (111) monochromator ($\Delta E/E = 5.4 \times 10^{-5}$ fwhm energy bandpass) and focused to a fwhm spot size of 5 $\mu$m × 5 $\mu$m using Kirkpatrick Baez mirrors. The standard 24 bunch operating mode of the APS was used which provides evenly spaced X-ray pulses at 6.52 MHz with 153 ns separation. The laser (Duetto, Time Bandwidth) was synchronized to the X-rays through the storage ring rf. The laser's repetition rate was 3.26 MHz, and pulses were set to overlap every other X-ray pulse at the sample with a 100 ps delay. The second harmonic of the Duetto laser was used (532 nm) which had a 10 ps pulse duration. The incident laser power was 2 W, and fluence on the sample was ≈30 mJ/cm$^2$. The laser spot size was approximately 6 times larger than the X-ray spot and carefully aligned to the X-ray beam so that the X-rays probed only the sample volume with the highest excitation fraction. The flow speed of the jet was ∼6 m/s which was not fast enough to refresh the probed volume for each pump−probe cycle. However, the sample was known to recover completely back to the ground state within less than 5 ns which was considerably faster than the 306 ns pump−probe cycle period. The detector was run in gating mode,[25] accumulating signal only during ∼100 ns intervals around every other X-ray pulse at a 3.26 MHz repetition rate for ≈12 s before an image was read-out. The position of the gate in time was alternated between overlap of the signal from laser-pumped sample and from the ground-state sample between each image collection. The total acquisition time for the emission spectrum was 19 h. Spectra were normalized to the area under the curves so that potential artifacts such as variations in jet thickness, density decrease (due to thermal expansion), and concentration changes were accounted for.

**Computational Details.** All calculations were carried out using the ORCA 3.0 quantum chemistry package[26] using density functional theory. We used the B3LYP* functional (the standard B3LYP[27−29] hybrid functional reparametrized by Reiher[30]), in combination with the TZVP basis set.[31] The structures for the LS and HS states of $[Fe(terpy)_2]^{2+}$ were fully


DOI: 10.1021/acs.jpcc.6b12940
J. Phys. Chem. C 2017, 121, 2620−2626

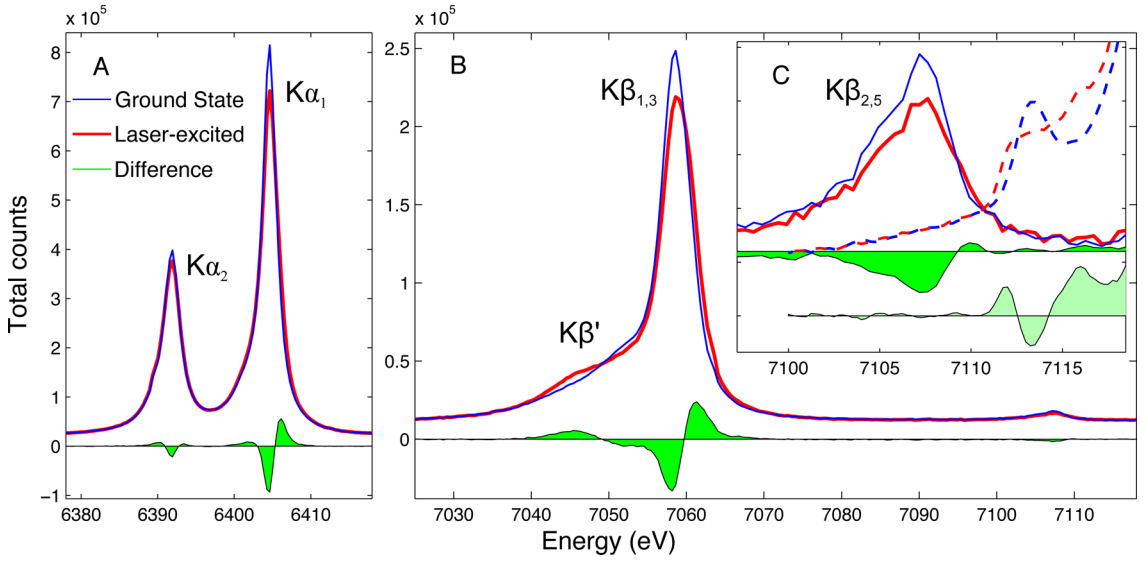


**Figure 2.** Full 1s XES of $[Fe(terpy)_2]^{2+}$; blue (thin) lines denote spectra of the ground state, red (thick) lines denote data measured 100 ps after laser excitation, and the green filled areas show the spectral variation. (A) The K$\alpha$ region. (B) The mainline K$\beta$ and vtc-XES regions. (C) The inset shows the contributions from the region of the frontier orbitals: the K$\beta_{2,5}$ region of vtc-XES maps the highest occupied MOs, while the 1s X-ray absorption pre-edge (dashed lines) projects the lowest unoccupied MOs.

optimized, and the vtc-XES was calculated in a quasi one-electron picture,[2,3] applying the implementation of Neese and co-workers.[5,6] The numerical integration accuracy was set to 7.0 for the Fe atom in order to achieve a more accurate description. The modeled spectra were broadened with a pseudo-Voigt line profile, in order to account for broadenings from the core-hole lifetime and the experimental resolution. Full widths at half-maximum (fwhm) of 1.4 eV for the Lorentzian and 1.5 eV for the Gaussian component were chosen to achieve agreement with the experimental spectra.

## RESULTS AND DISCUSSION

The measured XES spectra for aqueous $[Fe(terpy)_2]^{2+}$ in its LS ground and laser-pumped excited states are shown in Figure 2 together with their difference spectra. The emission lines reflecting core-to-core transitions include the K$\alpha_1$ ($2p_{3/2} \rightarrow 1s$) and K$\alpha_2$ ($2p_{1/2} \rightarrow 1s$) peaks in Figure 2A and the K$\beta_{1,3}$ peak and K$\beta'$ shoulder ($3p \rightarrow 1s$) in Figure 2B. These emission lines do not directly probe the valence electron structure but are quite sensitive to the spin density of the central metal ion. This stems from the intra-atomic exchange interaction in the final state of the emission process between the unpaired electrons in the metal-centered 3d orbitals and the 2p or 3p core-hole. The unpaired d electrons in the HS state lead to a broadening of the K$\alpha_1$ and K$\alpha_2$ lines, next to a blue shift of the K$\beta_{1,3}$ line, and an intensity transfer from the K$\beta_{1,3}$ peak to the K$\beta'$ satellite.[11,32−34] The spectral changes observed in Figure 2 reflect the expected transition from LS to HS,[22,34,35] in agreement with our previous time-resolved core-to-core XES measurements on the same compound.[18]

The vtc-XES region is found on the high energy side of the K$\beta_{1,3}$ peak in Figure 2B and is shown magnified by a factor of 22 in Figure 2C. Although it is much weaker than the core-to-core emission lines (200 times smaller than the dominating K$\alpha_1$ line), vtc-XES is valuable because it directly reflects occupied valence orbitals. The peak observed in Figure 2C, historically referred to as K$\beta_{2,5}$, has been shown in 3d transition metal complexes to be dominated by contributions from highest occupied valence orbitals that have mixed metal p and ligand p character.[5,9] The K$\beta_{2,5}$ peak in the laser-excited vtc-XES spectrum is reduced in intensity and slightly shifted to higher energy relative to the LS ground state, and the origins of these changes will be discussed in what follows. Figure 2C also shows the pre-edge X-ray absorption spectra (XAS) for ground-state and laser-excited $[Fe(terpy)_2]^{2+}$, which have been previously measured and theoretically described[18] and that reflect transitions from the Fe 1s orbital to lowest *unoccupied* orbitals that contain metal d character.[11,36] The LS ground state has only a single resonance while population variations due to a smaller ligand field leads to the appearance of three resonances in the laser-pumped pre-edge XAS spectrum.[18,37] The ability to now record both vtc-XES and pre-edge XAS in time-resolved measurements promises a more comprehensive picture of the changes in the frontier orbitals that occur as reactions proceed.

Figure 3 shows the measured vtc-XES spectra compared to theory. It has been found that one-electron descriptions can provide excellent results for vtc-XES spectra (apart from the absolute energies).[3,5,6,8,38−40] These DFT calculations capture the vtc-XES features in general, very well, and this also holds for our case. The magnitudes of the intensity reduction and blue energy shift calculated for the HS state relative to the LS state (red and blue lines, respectively, in Figure 3A) are larger than what is observed in the measurement, which is due to the fact that the measured laser-excited spectrum (red line in Figure 3B) consists of a mixture of LS and HS molecules. The estimated excitation fraction for the measurement, based on an analysis of the measured changes in the mainline K$\beta$ spectrum, as described in previous work,[18] is 30%. Taking this fraction into account in the theoretical spectrum (red dashed line in Figure 3A), it is seen that the agreement with the experiment is good. The experimental difference is negative across the 7085−7100 eV (K$\beta''$) energy region and through the main K$\beta_{2,5}$ peak in agreement with the theoretical curve. A very small positive peak in the experimental difference on the high energy side of the K$\beta_{2,5}$ is observed, which is indicative of the blue shift predicted by theory. The assignment of this feature as a blue shift is further supported by comparison to statically measured


DOI: 10.1021/acs.jpcc.6b12940
J. Phys. Chem. C 2017, 121, 2620−2626

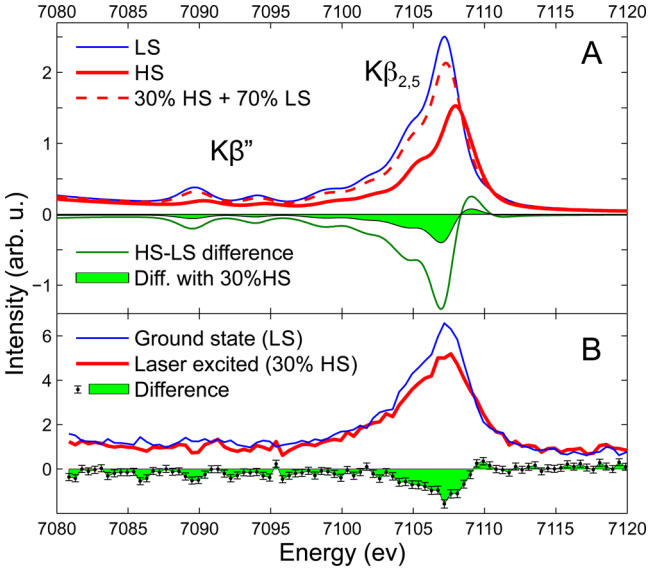


**Figure 3.** Calculated (A) and measured (B) vtc-XES spectra of LS and HS $[Fe(terpy)_2]^{2+}$. The theoretical curves correspond to 100% transition and have been shifted by +158 eV to match the experiment.

LS and HS spectra of a very similar Fe(II) complex, $[Fe(phen)_2(NCS)_2]$. In this complex the spin transition was induced by a temperature change and the spectra could be measured with better statistics. Figure 4 shows the LS singlet state and the HS quintet state of $[Fe(phen)_2(NCS)_2]$ along with their difference. The green-filled area corresponds to the difference reduced to 30%, the fraction of HS species in the $[Fe(terpy)_2]^{2+}$ time-resolved measurement. The structureless negative bleach signal and a very weak positive peak around

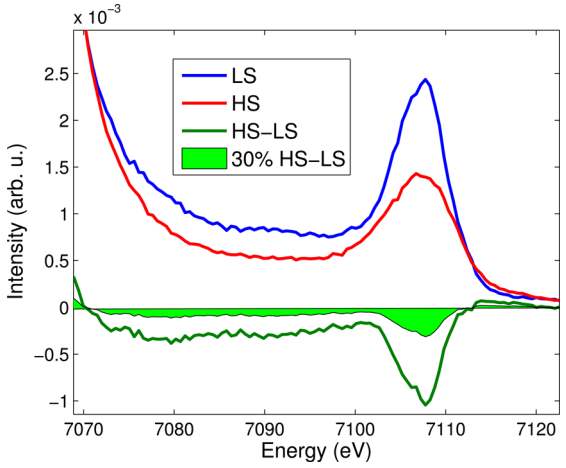


**Figure 4.** Statically measured vtc-XES of the LS (blue line) and HS (red line) states of $[Fe(phen)_2(NCS)_2]$. This Fe(II) complex is in many respects similar to $[Fe(terpy)_2]^{2+}$, but due to the smaller ligand field splitting the spin transition could be induced by a temperature change (rather than by light), and the HS state is stable above a certain temperature. The LS singlet state is very similar to the ground state of $[Fe(terpy)_2]^{2+}$, and the HS quintet state is comparable to the excited state of $[Fe(terpy)_2]^{2+}$. The dark green line is the difference between the LS and HS states, and the green filled area corresponds to the difference reduced to 30%, which is the fraction of HS species in the time-resolved measurement on $[Fe(terpy)_2]^{2+}$. Reproduced from the data in Figure 1 in G. Vankó et al. *J. Phys. Chem. B* **2006**, *110*, 11647–11653.

7110 eV are found to be similar to those in the time-resolved measurement in Figure 3B.

The theoretical spectra yield insight into the origin of the experimental features, and examination of the calculations will constitute the remainder of this discussion. Figure 5 presents

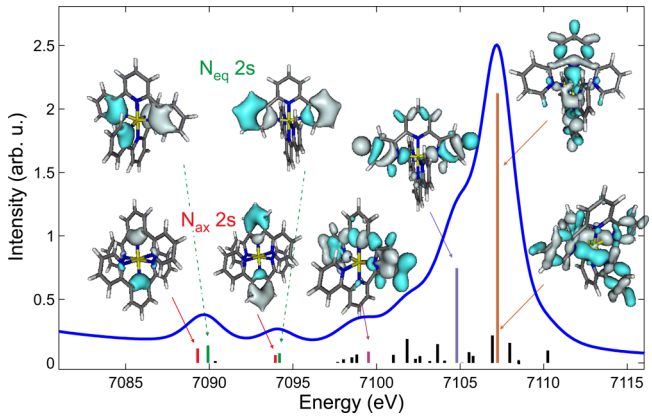


**Figure 5.** Molecular orbital contributions to the vtc-XES spectra of LS $[Fe(terpy)_2]^{2+}$. In the so-called K$\beta''$ region, contributions from the N 2s-based molecular orbitals are unambiguously identified. Above 7095 eV (K$\beta_{2,5}$) MOs stemming from N 2p mixed with iron orbitals make up the spectra.

details of the calculated LS spectrum. Oscillator strengths for each vtc emission line are represented by a so-called stick spectrum, and the blue line represents the envelope obtained when broadening accounting for the core-hole lifetime and experimental resolution is introduced. Representations of the most relevant molecular orbitals (MOs) contributing to the spectral features are shown. Dipole-allowed transitions dominate the vtc-XES, so MOs with Fe p character are the primary contributors to the spectrum. In complexes such as $[Fe(terpy)_2]^{2+}$, the orbitals with metal p mixing have mostly ligand character. We find that MOs with ligand 2s character contribute at lower energy (the K$\beta''$ part of the spectrum), and MOs with ligand 2p character contribute to the K$\beta_{2,5}$ region, consistent with previous assignments.[1]

The K$\beta''$ region is often simpler to interpret than the K$\beta_{2,5}$ because the energies of features are characteristic of the donor atom within the ligand. In the present case the two peaks observed in the calculations at 7090 and 7094 eV in Figure 5 could be naively assigned to transitions involving 2s orbitals from the two more tightly bound axial nitrogen atoms ($N_{ax}$, $R(N_{ax}–Fe)$ = 1.886 Å) and the four more loosely bound equatorial nitrogen atoms ($N_{eq}$, $R(N_{eq}–Fe)$ = 1.985 Å) that are present in $[Fe(terpy)_2]^{2+}$.[18] Their energy separation is expected because a smaller bond length for the axial ligand atoms, thus larger metal–ligand orbital overlap, stabilizes these MOs in energy, resulting in a higher binding energy and a correspondingly lower emission energy. Our calculations reveal, however, more complexity. An energy splitting between the emission lines involving $N_{ax}$ and $N_{eq}$ 2s orbitals is found (red vs green sticks, respectively, in Figure 5) but with much smaller magnitude than the peak separation. The two peaks in the vtc spectrum are found instead to result from two different kinds of MOs that involve ligand 2s orbitals: those with large N 2s orbital mixing coefficients (contributing to the lower energy peak) and those with substantial C 2s (and to some smaller extent C 2p) orbital mixing alongside N 2s mixing that


DOI: 10.1021/acs.jpcc.6b12940
J. Phys. Chem. C 2017, 121, 2620–2626

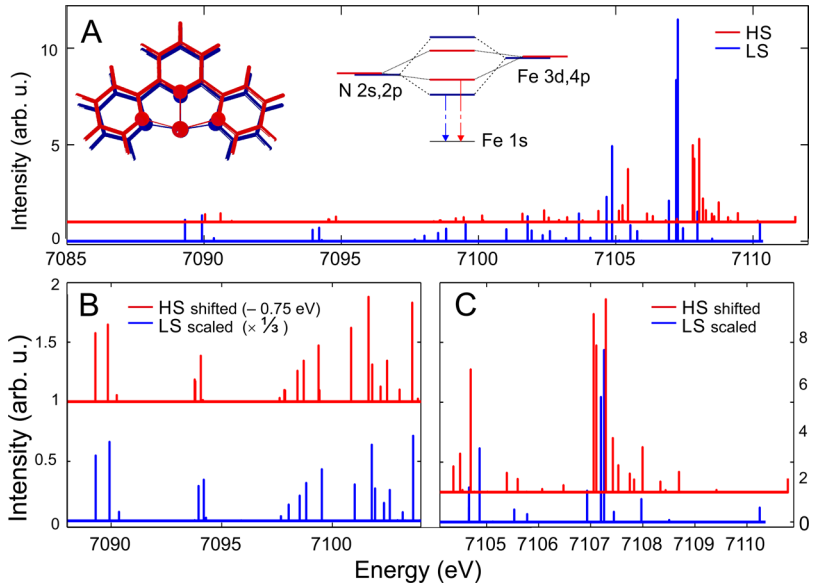


**Figure 6.** (A) Stick diagram of the molecular orbital contributions to the vtc-XES spectra of LS and HS $[Fe(terpy)_2]^{2+}$ (blue and red, respectively). The variation of the molecular structure is also shown on an iron with a single terpy ligand. The expected variation of the orbital transition energies with the bonding length are also shown in a simple scheme. The bottom of the figure shows the vtc-XES spectra with the HS shifted by −0.75 eV and the intensity of the LS divided by 3 for better comparison. (B) The lower energy part reveals that the lower-lying bonding orbitals are rather similar in the two states, only affected by the change in the overlap of the orbitals, reflected by the energy shift and the intensity change. (C) The higher energy region, on the other hand, is directly affected by the change in the orbital populations.

contribute to the higher energy peak. This result exemplifies the sensitivity of vtc-XES to intricate details of the valence electronic structure.

The origin of the experimentally observed blue shift and amplitude reduction can be understood by examining the calculated LS and HS spectra in Figure 6. Figure 6A shows stick spectra for the two states, with the HS spectrum vertically offset for clarity. The reduction in amplitude and shift to higher energy in the HS spectrum are found to be constant across a large portion of the spectral range. This can be seen in Figures 6B and 6C where the HS spectrum has been shifted by −0.75 eV and the amplitude of the LS spectrum has been divided by 3. Once the energy shift and intensity reduction have been removed, the positions and intensities of the transitions are seen to be very similar between LS and HS, particularly in the lower energy part shown in Figure 6B. As explained earlier and indicated in the schematic in Figure 6A, the blue energy shift indicates a destabilization of the probed MOs. This is expected for the spin-state transition because two of the six Fe 3d electrons originally residing in the nonbonding $t_{2g}$ orbitals (in the LS state) now populate antibonding $e_g^*$ orbitals in the HS state, and this causes the elongation of the Fe-ligand bonds, diminishing orbital overlap. Time-resolved EXAFS measurements revealed an increase of 0.2 Å for the $N_{ax}$−Fe bonds and 0.23 Å for the $N_{eq}$−Fe bonds.[18] The reduction in intensity from LS to HS indicates that the amount of Fe p character contributing to the populated MOs has decreased, which implies that some electron density has moved from the Fe to the ligand. This observation is similar to recent findings by Van Kuiken et al.[41] where time-resolved XAS at the N K-edge was used to study a similar Fe complex. A shift to lower energy of the N absorption peak originating from a N 1s → ligand $\pi^*$ transition was interpreted as arising from more negative charge at the N sites. Our calculations reveal that vtc-XES is sensitive to the electron population and density at the Fe center and can complement N XAS in its sensitivity to electron density at the ligands.

The measured $K\beta_{2,5}$ feature is on the higher energy side of the spectrum and should be compared to the calculations in Figure 6C. In this region, an overall blue shift of approximately 0.75 eV is present but alongside more subtle changes in the positions of the emission lines and the appearance of new lines at the highest energies. Additionally, there is more variation in the intensity reduction in individual lines. These observations are indicative of the fact that this region reflects occupied MOs that are more affected by changes of the electron populations in the frontier orbitals. In particular, the new lines at the high-energy side are found to be from MOs based on the mixing of Fe 3d and N 2p orbital, which have reduced symmetry that makes the vtc transitions dipole allowed. Their presence is a result of the lowered symmetry of the HS state ($C_2$ as opposed to $D_{2d}$ in the LS state). These orbitals include the highest occupied MOs in the HS state, the $e_g^*$ orbitals populated at the spin-state transition. The experimentally observed intensity reduction and blue shift, then, is understood to be due to the reduced metal−ligand orbital overlap in combination with the appearance of new emission lines reflecting differently populated orbitals in the HS state.

The calculated spectra presented here contain finer details not yet detectable in the measured spectra, indicating that an improvement in the signal-to-noise (S/N) ratio would be beneficial. More X-ray flux would help here. We performed our measurements using monochromatic X-rays, but vtc-XES can benefit from broader bandwidth incident X-rays. For example, at 7ID-D of the APS, so-called "pink beam" operation with ∼1% bandwidth would provide ∼100 times more X-ray flux. XFEL facilities, such as European XFEL and LCLS-II-HE, will provide $10^4$ times more flux than used here, enabling high S/N vtc-XES spectra.

The information extractable from vtc-XES is comparable to that obtained from photoelectron spectroscopy because the


DOI: 10.1021/acs.jpcc.6b12940
J. Phys. Chem. C 2017, 121, 2620−2626

final states in both processes are the same, with a hole in the valence orbitals. Vtc-XES provides element selectivity, and as a hard X-ray photon-in/photon-out technique, it offers a large sampling depth and can thus be implemented with very different sample environments (e.g., free-flowing liquid jets, in situ and/or operando catalytic reactors, etc.). These advantages make vtc-XES a promising means for gaining access to valence electronic structure for presently challenging systems.

## CONCLUSION

We have measured the complete Fe 1s emission spectrum of photoexcited $[Fe(terpy)_2]^{2+}$ in solution, capturing the transient, photoinduced singlet to quintet spin-state change in the K$\alpha$ and mainline K$\beta$ emission lines as well as the corresponding valence orbital changes in the vtc emission. This is, to the best of our knowledge, the first proper vtc-XES measurement (and the first full 1s XES) made with picosecond temporal resolution. The vtc-XES of the transient HS state is found to be reduced in intensity and shifted slightly to higher energy. DFT calculations capture the experimental spectral changes well. The intensity reduction is understood to be a result of the expansion of the Fe−ligand bonds; photoexcitation leads to population of antibonding orbitals which causes elongation of the Fe−ligand bonds, loss of Fe-ligand orbital overlap, and therefore reduction of the Fe p MO character that contributes to the vtc emission lines. The energy shift is also expected from the bond elongation; the blue shift indicates a destabilization of the probed MOs, a result of the diminished orbital overlap. Further analysis of the DFT calculated vtc-XES spectra indicates that fine details in the K$\beta''$ region hold more information about the valence MO structure. Additionally, calculations reveal that newly populated MOs in the HS state contribute to the high energy side of the K$\beta_{2,5}$ vtc peak. While these finer features are difficult to observe in our present measured spectra due to the limited statistics, new experimental opportunities with X-ray sources providing higher flux, such as "pink beam" capability at synchrotrons and upcoming high-repetition-rate XFELs, promise to enable more detailed experimental observations. Time-resolved vtc-XES offers a means of directly monitoring photoinduced changes in the valence orbitals, those directly involved in photoinitiated dynamics, with penetration power and elemental specificity. Combined with other hard X-ray techniques, such as EXAFS, vtc-XES can be used to correlate valence orbital changes with geometric changes for a wide variety of systems.

## AUTHOR INFORMATION


### Corresponding Authors

*E-mail: amarch@anl.gov.
*E-mail: wojciech.gawelda@xfel.eu.
*E-mail: vanko.gyorgy@wigner.mta.hu

### ORCID

Anne Marie March: 0000-0003-2961-1246
György Vankó: 0000-0002-3095-6551


### Notes

The authors declare no competing financial interest.

## ACKNOWLEDGMENTS

Work by A.M.M., G.D., S.H.S., and L.Y. was supported by the U.S. Department of Energy (DOE), Office of Science, Basic Energy Sciences (BES), Chemical Sciences, Geosciences, and Biosciences Division. Z. N., P.M., and G. V. were supported by the 'Lendület' (Momentum) Program of the Hungarian Academy of Sciences (LP2013-59), the European Research Council via contract ERC-StG-259709 (X-cited!), and the Hungarian Scientific Research Fund (OTKA) under contract K29724. Z.N. acknowledges support from the Bolyai Fellowship of the Hungarian Academy of Sciences. P.M. acknowledges support from the People Programme (Marie Curie Actions) of the European Union's Seventh Framework Programme (FP7/2007-2013) under REA grant agreement no. 609405 (COFUNDPostdocDTU). T.A.A., C.B., C. Bressler, A.B., M.D., A.G., D.K., S.S., and W.G. acknowledge funding by the Hamburg Centre of Ultrafast Imaging (CUI), the Deutsche Forschungsgemeinschaft via SFB 925/A4, the European XFEL GmbH, and the European Cluster of Advanced Laser Light Sources (EUCALL) via the Horizon 2020 Research and Innovation Programme under grant agreement no. 654220. This research used resources of the Advanced Photon Source, a U.S. Department of Energy (DOE) Office of Science User Facility operated for the DOE Office of Science by Argonne National Laboratory under contract no. DE-AC02-06CH11357. We are grateful to the staff of 7-ID from the APS for help during the experiment.

## REFERENCES


(1) Bergmann, U.; Horne, C. R.; Collins, T. J.; Workman, J. M.; Cramer, S. P. Chemical Dependence of Interatomic X-ray Transition Energies and Intensities − A Study of Mn K$\beta''$ and K$\beta_{2,5}$ Spectra. *Chem. Phys. Lett.* **1999**, *302*, 119−124.

(2) Bergmann, U.; Bendix, J.; Glatzel, P.; Gray, H. B.; Cramer, S. P. Anisotropic Valence → Core X-ray Fluorescence from a $[Rh(en)_3]$-$[Mn(N)(CN)_5]\cdot H_2O$ Single Crystal: Experimental Results and Density Functional Calculations. *J. Chem. Phys.* **2002**, *116*, 2011−2015.

(3) Smolentsev, G.; Soldatov, A. V.; Messinger, J.; Merz, K.; Weyhermüller, T.; Bergmann, U.; Pushkar, Y.; Yano, J.; Yachandra, V. K.; Glatzel, P. X-ray Emission Spectroscopy To Study Ligand Valence Orbitals in Mn Coordination Complexes. *J. Am. Chem. Soc.* **2009**, *131*, 13161−13167.

(4) Safonov, V. A.; Vykhodtseva, L. N.; Polukarov, Y. M.; Safonova, O. V.; Smolentsev, G.; Sikora, M.; Eeckhout, S. G.; Glatzel, P. Valence-to-Core X-ray Emission Spectroscopy Identification of Carbide Compounds in Nanocrystalline Cr Coatings Deposited from Cr(III) Electrolytes Containing Organic Substances. *J. Phys. Chem. B* **2006**, *110*, 23192−23196.

(5) Lee, N.; Petrenko, T.; Bergmann, U.; Neese, F.; DeBeer, S. Probing Valence Orbital Composition with Iron K$\beta$ X-ray Emission Spectroscopy. *J. Am. Chem. Soc.* **2010**, *132*, 9715−9727.

(6) Pollock, C. J.; DeBeer, S. Valence-to-Core X-ray Emission Spectroscopy: A Sensitive Probe of the Nature of a Bound Ligand. *J. Am. Chem. Soc.* **2011**, *133*, 5594−5601.

(7) Lancaster, K. M.; Roemelt, M.; Ettenhuber, P.; Hu, Y.; Ribbe, M. W.; Neese, F.; Bergmann, U.; DeBeer, S. X-ray Emission Spectroscopy Evidences a Central Carbon in the Nitrogenase Iron-Molybdenum Cofactor. *Science* **2011**, *334*, 974−977.

(8) Pollock, C. J.; DeBeer, S. Insights into the Geometric and Electronic Structure of Transition Metal Centers from Valence-to-Core X-ray Emission Spectroscopy. *Acc. Chem. Res.* **2015**, *48*, 2967−2975.

(9) Gallo, E.; Glatzel, P. Valence to Core X-ray Emission Spectroscopy. *Adv. Mater.* **2014**, *26*, 7730−7746.

(10) Bauer, M. HERFD-XAS and Valence-to-Core-XES: New Tools to Push the Limits in Research with Hard X-rays? *Phys. Chem. Chem. Phys.* **2014**, *16*, 13827−13837.

(11) Glatzel, P.; Bergmann, U. High Resolution 1s Core Hole X-ray Spectroscopy in 3d Transition Metal Complexes—Electronic and Structural Information. *Coord. Chem. Rev.* **2005**, *249*, 65−95.




DOI: 10.1021/acs.jpcc.6b12940
J. Phys. Chem. C 2017, 121, 2620−2626

(12) Pollock, C. J.; Grubel, K.; Holland, P. L.; DeBeer, S. Experimentally Quantifying Small-Molecule Bond Activation Using Valence-to-Core X-ray Emission Spectroscopy. *J. Am. Chem. Soc.* **2013**, *135*, 11803−11808.
(13) Pushkar, Y.; Long, X.; Glatzel, P.; Brudvig, G.; Dismukes, G.; Collins, T.; Yachandra, V.; Yano, J.; Bergmann, U. Direct Detection of Oxygen Ligation to the Mn(4)Ca Cluster of Photosystem II by X-ray Emission Spectroscopy. *Angew. Chem., Int. Ed.* **2010**, *49*, 800−803.
(14) Safonova, O. V.; Florea, M.; Bilde, J.; Delichere, P.; Millet, J. M. M. Local Environment of Vanadium in V/Al/O-Mixed Oxide Catalyst for Propane Ammoxidation: Characterization by In Situ Valence-to-Core X-ray Emission Spectroscopy and X-ray Absorption Spectroscopy. *J. Catal.* **2009**, *268*, 156−164.
(15) Günter, T.; Doronkin, D. E.; Boubnov, A.; Carvalho, H. W. P.; Casapu, M.; Grunwaldt, J.-D. The SCR of NOx with $NH_3$ Examined by Novel X-ray Emission and X-ray Absorption Methods. *Top. Catal.* **2016**, *59*, 866−874.
(16) McCusker, J. K.; Walda, K. N.; Dunn, R. C.; Simon, J. D.; Magde, D.; Hendrickson, D. N. Subpicosecond $^1$MLCT → $^5T_2$ Intersystem Crossing of Low-Spin Polypyridyl Ferrous Complexes. *J. Am. Chem. Soc.* **1993**, *115*, 298−307.
(17) Brady, C.; McGarvey, J. J.; McCusker, J. K.; Toftlund, H.; Hendrickson, D. N. Time-Resolved Relaxation Studies of Spin Crossover Systems in Solution. *Top. Curr. Chem.* **2004**, *235*, 1−22.
(18) Vankó, G.; Bordage, A.; Pápai, M.; Haldrup, K.; Glatzel, P.; March, A. M.; Doumy, G.; Britz, A.; Galler, A.; Assefa, T. A.; et al. Detailed Characterization of a Nanosecond-lived Excited State: X-Ray and Theoretical Investigation of the Quintet State in Photoexcited $[Fe(terpy)_2]^{2+}$. *J. Phys. Chem. C* **2015**, *119*, 5888−5902.
(19) Walko, D. A.; Adams, B. W.; Doumy, G.; Dufresne, E. M.; Li, Y.; March, A. M.; Sandy, A. R.; Wang, J.; Wen, H.; Zhu, Y. Developments in Time-Resolved Research at APS Beamline 7ID. *AIP Conf. Proc.* **2015**, *1741*, 030048.
(20) March, A. M.; Stickrath, A.; Doumy, G.; Kanter, E. P.; Krässig, B.; Southworth, S. H.; Attenkofer, K.; Kurtz, C. A.; Chen, L. X.; Young, L. Development of High-Repetition-Rate Laser Pump/X-ray Probe Methodologies for Synchrotron Facilities. *Rev. Sci. Instrum.* **2011**, *82*, 073110.
(21) Haldrup, K.; Vankó, G.; Gawelda, W.; Galler, A.; Doumy, G.; March, A. M.; Kanter, E. P.; Bordage, A.; Dohn, A.; van Driel, T. B.; et al. Guest-Host Interactions Investigated by Time-Resolved X-ray Spectroscopies and Scattering at MHz Rates: Solvation Dynamics and Photoinduced Spin Transition in Aqueous $Fe(bipy)_3^{2+}$. *J. Phys. Chem. A* **2012**, *116*, 9878−9887.
(22) Vankó, G.; Bordage, A.; Glatzel, P.; Gallo, E.; Rovezzi, M.; Gawelda, W.; Galler, A.; Bressler, C.; Doumy, G.; March, A. M.; et al. Spin-State Studies with XES and RIXS: From Static to Ultrafast. *J. Electron Spectrosc. Relat. Phenom.* **2013**, *188*, 166−171.
(23) Bressler, C.; Galler, A.; Gawelda, W. *Technical Design Report: Scientific Instrument FXE*. doi: 10.3204/XFEL.EU/TR-2012-008.
(24) Alonso Mori, R.; Kern, J.; Sokaras, D.; Weng, T.-C.; Nordlund, D.; Tran, R.; Montanez, P.; Delor, J.; Yachandra, V. K.; Yano, J.; et al. A Multi-Crystal Wavelength Dispersive X-ray Spectrometer. *Rev. Sci. Instrum.* **2012**, *83*, 073114.
(25) Ejdrup, T.; Lemke, H. T.; Haldrup, K.; Nielsen, T. N.; Arms, D. A.; Walko, D. A.; Miceli, A.; Landahl, E. C.; Dufresne, E. M.; Nielsen, M. M. Picosecond Time-Resolved Laser Pump/X-ray Probe Experiments Using a Gated Single-Photon-Counting Area Detector. *J. Synchrotron Radiat.* **2009**, *16*, 387−390.
(26) Neese, F. The ORCA Program System. *WIREs Comput. Mol. Sci.* **2012**, *2*, 73−78.
(27) Lee, C.; Yang, W.; Parr, R. G. Development of the Colle-Salvetti Correlation-Energy Formula into a Functional of the Electron Density. *Phys. Rev. B: Condens. Matter Mater. Phys.* **1988**, *37*, 785−789.
(28) Becke, A. D. Density-Functional Thermochemistry. III. The Role of Exact Exchange. *J. Chem. Phys.* **1993**, *98*, 5648−5652.
(29) Stephens, P. J.; Devlin, F. J.; Chabalowski, C. F.; Frisch, M. J. Ab Initio Calculation of Vibrational Absorption and Circular Dichroism Spectra Using Density Functional Force Fields. *J. Phys. Chem.* **1994**, *98*, 11623−11627.
(30) Reiher, M.; et al. Reparametrization of Hybrid Functionals Based on Energy Differences of States of Different Multiplicities. *Theor. Chem. Acc.* **2001**, *107*, 48−55.
(31) Schäfer, A.; Huber, C.; Ahlrichs, R. Fully Optimized Contracted Gaussian Basis Sets of Triple Zeta Valence Quality for Atoms Li to Kr. *J. Chem. Phys.* **1994**, *100*, 5829−5835.
(32) Peng, G.; de Groot, F.; Hämäläinen, K.; Moore, J.; Wang, X.; Grush, M.; Hastings, J.; Siddons, D.; Amstrong, W.; Mullins, O.; et al. High-Resolution Manganese X-ray Fluorescence Spectroscopy. Oxidation State and Spin-State Sensitivity. *J. Am. Chem. Soc.* **1994**, *116*, 2914−2920.
(33) Wang, X.; de Groot, F. M. F.; Cramer, S. P. Spin-Polarized X-ray Emission of 3*d* Transition-Metal Ions: A Comparison via K$\alpha$ and K$\beta$ Detection. *Phys. Rev. B: Condens. Matter Mater. Phys.* **1997**, *56*, 4553−4564.
(34) Vankó, G.; Neisius, T.; Molnár, G.; Renz, F.; Kárpáti, S.; Shukla, A.; de Groot, F. M. F. Probing the 3d Spin Momentum with X-ray Emission Spectroscopy: The Case of Molecular Spin Transitions. *J. Phys. Chem. B* **2006**, *110*, 11647−11653.
(35) Vankó, G.; Glatzel, P.; Pham, V.-T.; Abela, R.; Grolimund, D.; Borca, C. N.; Johnson, S. L.; Milne, C. J.; Bressler, C. Picosecond Time-Resolved X-Ray Emission Spectroscopy: Ultrafast Spin-State Determination in an Iron Complex. *Angew. Chem., Int. Ed.* **2010**, *49*, 5910−5912.
(36) de Groot, F.; Vankó, G.; Glatzel, P. The 1s X-ray Absorption Pre-Edge Structures in Transition Metal Oxides. *J. Phys.: Condens. Matter* **2009**, *21*, 104207.
(37) Westre, T. E.; Kennepohl, P.; DeWitt, J. G.; Hedman, B.; Hodgson, K. O.; Solomon, E. I. A Multiplet Analysis of Fe K-Edge 1s → 3d Pre-Edge Features of Iron Complexes. *J. Am. Chem. Soc.* **1997**, *119*, 6297−6314.
(38) Beckwith, M. A.; Roemelt, M.; Collomb, M.-N.; DuBoc, C.; Weng, T.; Bergmann, U.; Glatzel, P.; Neese, F.; DeBeer, S. Manganese K$\beta$ X-ray Emission Spectroscopy As A Probe of Metal−Ligand Interactions. *Inorg. Chem.* **2011**, *50*, 8397−8409.
(39) Delgado-Jaime, M. U.; DeBeer, S.; Bauer, M. Valence-to-Core X-Ray Emission Spectroscopy of Iron-Carbonyl Complexes: Implications for the Examination of Catalytic Intermediates. *Chem. - Eur. J.* **2013**, *19*, 15888−15897.
(40) March, A. M.; Assefa, T. A.; Bressler, C.; Doumy, G.; Galler, A.; Gawelda, W.; Kanter, E. P.; Németh, Z.; Pápai, M.; Southworth, S. H.; et al. Feasibility of Valence-to-Core X-ray Emission Spectroscopy for Tracking Transient Species. *J. Phys. Chem. C* **2015**, *119*, 14571−14578.
(41) Van Kuiken, B. E.; Cho, H.; Hong, K.; Khalil, M.; Schoenlein, R. W.; Kim, T. K.; Huse, N. Time-Resolved X-ray Spectroscopy in the Water Window: Elucidating Transient Valence Charge Distributions in an Aqueous Fe(II) Complex. *J. Phys. Chem. Lett.* **2016**, *7*, 465−470.


DOI: 10.1021/acs.jpcc.6b12940
*J. Phys. Chem. C* 2017, 121, 2620−2626